Nanoscale

Accepted Manuscript

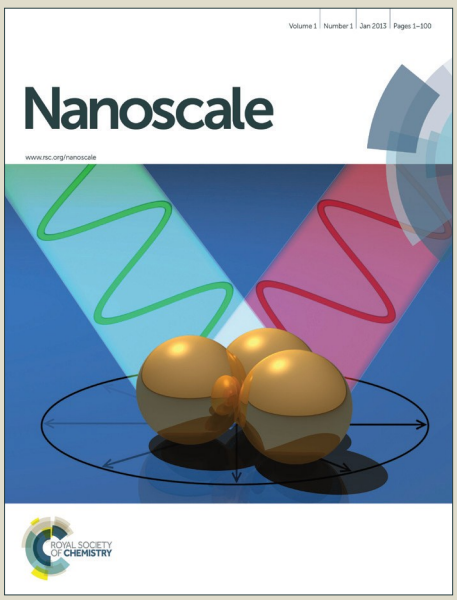

ROYAL SOCIETY OF CHEMISTRY

www.rsc.org/nanoscale

Nanoscale

RSCPublishing

ARTICLE

Surface charge effects in protein adsorption on nanodiamonds

Cite this: DOI: 10.1039/x0xx00000x

M. Aramesh [*a,c], O. Shimoni [b], K. Ostrikov [b,c,d], S. Prawer [a] and J. Cervenka [a]

Received 00th January 2012,
Accepted 00th January 2012

DOI: 10.1039/x0xx00000x

www.rsc.org/

Understanding the interaction of proteins with charged diamond nanoparticles is of fundamental importance for diverse biomedical applications. Here we present a thorough study of protein binding, adsorption kinetics and structure on strongly positively (hydrogen-terminated) and negatively (oxygen-terminated) charged nanodiamond particles using a quartz crystal microbalance with dissipation and infrared spectroscopy. By using two model proteins (bovine albumin serum and lysozyme) with different properties (charge, molecular weight and rigidity), the main driving mechanism responsible for the protein binding to the charged nanoparticles was identified. Electrostatic interactions were found to dominate the protein adsorption dynamics, attachment and conformation. We developed a simple electrostatic model that can qualitatively explain the observed adsorption behaviour based on charge-induced pH modifications near the charged nanoparticle surfaces. In neutral conditions, the local pH around the positively and negatively charged nanodiamonds becomes very high (11-12) and low (1-3) respectively, which has a profound impact on the protein charge, hydration and affinity to the nanodiamonds. Small proteins (lysozyme) were found to form multilayers with significant conformational changes to screen the surface charge, while larger proteins (albumin) formed monolayers with minor conformational changes. The findings of this study provide a step forward toward understanding and eventually predicting nanoparticle interactions with biofluids.

Introduction

Nanometer-sized diamond particles are emerging as new promising imaging agents and therapeutic carriers for biological and medical applications.[1-7] Nanodiamonds (NDs) integrate several unique properties, such as superior chemical and biological stability,[4] non-toxicity at both cellular and whole-organism levels [7-9] and ability to emit strong fluorescence after the introduction of defects.[1-3, 10] Furthermore, the ND surface can be chemically modified via diverse chemical routes to provide NDs with specific functionalities.[10, 11] This opens a range of opportunities for use of NDs in-vivo and in-vitro in targeted drug delivery and biosensor applications. However, when a material is inserted in a biological system its surface first interacts with freely diffusing biomolecules, such as proteins, enzymes and nucleic acids.

It is generally accepted that the interaction of proteins with a surface of a material plays a major role in determining the biocompatibility of the material and cell adhesion, growth and proliferation.[12] Previous studies have found that different surface chemistry and charge of nanoparticles can have a significant influence on the way how proteins interact with the nanoparticles.[13] The three dimensional structure of a protein is sensitive and small changes in its environment can induce a conformational change, which can affect its biological function.[14] For this reason good understanding of protein-nanodiamond interaction is essential.

During the past decades substantial progress has been made in understanding the mechanism of protein adsorption on different materials.[15-19] Proteins can be attached to a surface in diverse quantities, densities, conformations and orientations, depending on the chemical and physical properties of the material.[12, 13] Protein adsorption is a complex process involving electrostatic, hydrophobic, hydrogen bonding and van der Waals interactions. Additionally, the adsorption may also have a significant impact on the hydration layer, potentially changing the protein's structure and function,[12] Determination of the dominant interaction and its effect on the protein function is a long standing problem. However, this problem is challenging due to many inter-related mechanisms and complexity of the liquid/solid system. Despite several studies reported on the interaction of proteins with diamond surfaces[20, 21] and NDs,[22-24] the role of the surface chemistry and charge is still unclear.

The effects of charged ND particles on the adsorption of two model proteins, bovine albumin serum (BSA) and lysozyme (LYS), are investigated. BSA is the most abundant plasma protein in the circulatory system with negative surface charge at pH 7.0.[25, 26] On the other hand LYS is a positively charged protein of the immune system found in tears, saliva, and other secretions. We study how these two model proteins with different properties (size, charge and rigidity) interact with hydrogen- and oxygen-terminated surfaces of NDs in water.

Hydrogen- and oxygen-terminated NDs (H-ND and O-ND) represent well-defined chemical modifications of diamond surfaces with strong positive and negative charge in water, respectively. Quartz crystal microbalance with dissipation monitoring (QCM-D) and Fourier transform infrared spectroscopy (FTIR) are used to study the dynamic of the adsorption and conformational changes of the proteins on NDs. It is demonstrated that protein adsorption is strongly affected by ND charge. This result contradicts the common attraction/repulsion model using charged particles.

A more nuanced electrostatic model is presented that can qualitatively explain the main driving forces for protein attachment on charged ND surfaces. In particular, it is shown that electrostatic forces are effective in changing the local pH of the water interface close to the charged ND surfaces, strongly affecting the protein charge, adsorption dynamics, conformation and hydration. This study brings a new insight in the adsorption mechanism of proteins on charged nanoparticles (NDs).

Materials and Methods

Materials

Powders of detonation NDs (grade G01) were purchased from PlasmaChem GmbH. Surfaces of as-received NDs have been modified with oxygen and hydrogen to provide them with negative and positive charge in water as described elsewhere.[27] Oxygen-terminated NDs (O-ND) were obtained by annealing in oxygen gas with 99.999% purity at 600°C for 6 h. Hydrogen-terminated NDs (H-ND) were prepared by annealing the oxygen terminated powders in forming gas (4.07% H_2 in Ar) at 800°C for 16 h. Then the annealed ND powders were dispersed in Milli-Q water (resistance > 18 Ω) at concentration of 1 mg mL^{-1}. The solutions were ultrasonicated in a bath-sonicator for 0.5 h and centrifuged at 20,000 rcf for 6 h. The supernatants were extracted after the centrifugation and used for the protein-ND interaction study. The resulting ND solutions had pH of 7.0 and concentration of 0.3 ± 0.1 mg mL^{-1} (~ 30% of the original concentrations as calculated by measuring the mass of the dried remnant). Zeta potential and size measurements (Malvern Zetasizer, Nano ZS with a 633 nm laser) of the dispersed ND solutions showed that oxygen- and hydrogen-terminated NDs had an average nanoparticle size of 5±1 nm, with zeta potential of -51±2 and +49±2 mV respectively (Table 1). FTIR spectra of the NDs can be found in Supplementary Information (Fig. S1†).

BSA (bovine albumin serum) and LYS (from chicken egg white) were obtained from Sigma Aldrich and used as received. Protein solutions with 1 mg mL^{-1} concentrations were prepared using Milli-Q water as the solvent. HCl (1 M) and NaOH (1 M) were added adequately to adjust the pH of the solution to 7.0 at 25°C.

QCM-D

Real-time measurements of the adsorption were performed using a four-chamber QCM-D (E4, Q-Sense, Biolin Scientific, Sweden) and standard 50 nm thick SiO_2 coated sensors (QX303, ATA Scientific, Australia) with an effective surface area of 1 cm^2. A detailed description of the working principles of the QCM-D setup can be found elsewhere.[28] The QCM sensors were cleaned according to the standard cleaning protocol.[29] All the measurements were done using a constant flow rate of 20 µl min^{-1}. Prior to each experiment the chambers were flushed by Milli-Q water until the frequency of the sensors were stabilized (~20 min). The surface of the sensors was fully coated with NDs using a continuous flow of ND solutions for 1 h. In the consequent protein adsorption study, the ND-coated sensors were first rinsed with Milli-Q water, followed by a protein flow. Each sensor was used only once for each measurement. The temperature was fixed at 25°C during all measurements.

The Sauerbrey equation (Equation 1) was used to estimate the adsorbed mass on the QCM chip corresponding to the frequency shifts (Δf):

$$M = -C\frac{\Delta f}{n}, \quad (1)$$

where C is the mass sensitivity constant (17.7 ng cm^{-2} Hz^{-1} for 5 MHz crystals), and n is the overtone number. The third overtone (n = 3) was used for the analysis. The magnitude of the frequency shifts after rinsing with water (Δfdes) serves as an indicator of protein attachment strength, because the stronger the binding the harder to wash away [30]. It is important to note here that the values of the adsorbed mass in QCM-D correspond to wet mass due to the contribution of adsorbed water. In addition, simultaneous monitoring of Δf and dissipation changes (ΔD) allowed to obtain information about the viscoelastic and hydration effects and conformational changes of the proteins [28].

ATR-FTIR

Attenuated total reflectance Fourier transform infrared spectroscopy (ATR-FTIR) of the samples were acquired using a FTIR Bruker Tensor-27 spectrometer with a diamond crystal and resolution of 4 cm^{-1} by averaging the measurements over 16 scans. Samples were prepared by adding 200 µl of 1 mg mL^{-1} protein solution to 1 mL of 0.3 ± 0.1 mg mL^{-1} ND solutions. The ND-protein solutions were mixed at 25°C using a vortex mixer for 2 h. The mixed solutions were then centrifuged at 8,000 rcf for 5 min. The supernatants were removed and the products were rinsed with distilled water and centrifuged again. This step was repeated three times, after which pellets were collected and partially dried with a gentle nitrogen flow immediately before FTIR spectroscopy.

The measured FTIR spectra were smoothed by an average of 10 adjacent points and fitted using the fitting procedure reported in the literature.[31, 32] The spectra help interpreting the extent of conformation changes in the proteins. The amide I peaks were curve-fitted using the fitting parameters from the literature.[31, 32] The second derivatives of the curves were used to estimate the full width at half maximum (FWMH) of the peaks.

Results

ND adsorption on silica surface. Table 1 shows the properties of different types of NDs used in this study obtained

from dynamic light scattering (DLS) measurements. The oxygen-terminated (O-ND) and hydrogen-terminated (H-ND) nanodiamonds form stable monodispersed colloids in water due to their large negative and positive surface potentials, respectively.

Fig. 1 shows the adsorption profiles of O-ND and H-ND on SiO_2 surfaces of the QCM chips. The information obtained from the adsorption profile graphs is summarized in Table 2. The steep change in the QCM frequency (Fig. 1a) suggests that both H-ND and O-ND attach very quickly to the silica surface. The faster adsorption speed of H-ND compared to O-ND can be explained by an electrostatic attraction between negatively charged silica surface and positively charged H-ND. The bonding of the NDs to the surface of the silica is very strong, and the attached NDs cannot be removed from the surface by further water rinsing of the sensors.

The observed dissipation changes (ΔD) are relatively small for both types of NDs ($\Delta D_{O\text{-}ND}$ = 2.8, $\Delta D_{H\text{-}ND}$ = 2.04), indicating considerable rigidity of the formed NDs layers. The near-linear $\Delta D/\Delta f$ plot (Fig. 1c) shows that the ND reaction with the silica surface is a single-stage adsorption process. However, the adsorption dynamics $(\partial(\Delta f)/\partial t)$ comprises two accelerating and decelerating stages. The first accelerating stage is shorter than the second decelerating stage. NDs attach quickly to the silica surface in the first step (2 min for H-ND and 3 min for O-ND), due to a large number of available sites. At the decelerating part (5 and 6 min for H-ND and O-ND, respectively), the ND deposition slows down most probably because of the surface saturation by NDs and a competition for fewer available sites.

The calculated mass of the adsorbed NDs is 242 and 203 ng for H-NDs and O-NDs, respectively. The mass amounts correspond to $1.8\pm0.3 \times10^{12}$ and $1.5\pm0.3 \times10^{12}$ particles per 1 cm^2, respectively. Although this number is slightly larger than what is expected for fully packed ND monolayers on the surface, atomic force microscopy images of the surfaces suggest that the NDs form a close-packed monolayers on the QCM chips and the additional mass comes from adsorbed water. The as-deposited ND layers on QCM chips were used for the further protein adsorption studies.

It is worthwhile mentioning that the adsorption behaviour of larger NDs (50 nm) on QCM chips has been found completely different compared to the smaller detonation NDs (5 nm). The larger NDs did not attach to the silica QCM chips, even though they had the same zeta-potential. Moreover, their adsorption profiles showed many fluctuations in both frequency and dissipation (Fig. S2†). This result is most probably due to a different shape and a fabrication method of the larger NDs, which are used as abrasives. The spiky shape of ND abrasives can lead to a limited contact between sharp ND edges and the silica surface. This is why adsorption of 50 nm NDs cannot be accurately measured using QCM-D.

Protein adsorption on NDs. Fig. 2 shows QCM-D adsorption profiles of BSA and LYS on positively (H-ND) and negatively (O-ND) charged NDs. The extracted data is summarized in Table 3, which also shows the results for protein adsorption on clean SiO_2 QCM reference substrates. The adsorption profiles are very different for proteins and types of ND surface termination/charge. The Δf and ΔD profiles in Fig. 2 contain information about the kinetics of the reaction between the proteins and ND surfaces.

Adsorption equilibrium. The equilibrium conditions are reached when there are no more changes in frequency and energy dissipation. While the adsorption of BSA reaches an equilibrium stage shortly within 3-7 min, the adsorption process of LYS takes much longer (30 min on O-ND and more than 180 min on H-ND) and exhibits multiple adsorption events.

Amount of adsorbed proteins. The measured mass of adsorbed BSA is found almost equal for both ND surfaces (~ 3.5 ng mm^{-2}). The ratio of the number of adsorbed BSA to the number of the ND particles on the surface is 1.9±0.4 and 2.0±0.4 for O-ND and H-ND respectively.

In contrast, the amount of the adsorbed LYS strongly depends on the ND surface termination. The mass of the adsorbed LYS is 1.30 and 2.49 ng mm^{-2} on O-ND and H-ND surfaces, respectively. This corresponds to 3.0±0.4 and 6.8±0.4 of LYS per single O-ND and H-ND, respectively.

It should be stressed that the calculated mass is the wet mass of the proteins, which is usually larger than the dry mass.[19] A previous study of Ouberai *et al.* has reported that the mass of adsorbed BSA and LYS contains approximately 12-23% and 51-52% of water, respectively.[18] One can thus expect that the ratio between the number of adsorbed proteins to the number of ND particles to be smaller than that determined from the measured wet mass changes.

Binding strength. The binding affinity of the proteins to the NDs is qualitatively compared by the measured frequency shift upon rinsing with water (Fig. S3†). The binding affinity is expressed as Δf_{des} and ΔD_{des} in Table 3. BSA has a slightly higher affinity to H-ND compared to O-ND. On the other hand, LYS generally exhibits lower affinity for both types of NDs compared to BSA, with a larger frequency shift on H-ND after wash. The much lower affinity of LYS to H-ND is attributed to the formation of the multiple protein layers, as will be discussed later.

Adsorption speed. The first derivative of the frequency changes over time in QCM gives information related to the speed of protein adsorption. The LYS adsorption profile exhibits in general much slower adsorption rate compared to BSA (Fig. 2 a, d). Both BSA and LYS adsorb faster on O-ND (3.5 and 30 min) compared to H-ND (7 and 180 min). Similar to ND deposition on the silica surface, the adsorption of BSA (Fig. 2b) shows a first shorter accelerating stage (1.5 min) followed by a longer decelerating stage (2 min).

LYS adsorption shows a more complicated adsorption profile than BSA, exhibiting multiple adsorption events. The initial adsorption of LYS is relatively fast on O-ND and H-ND (2.5 min), while the following LYS adsorption stages are much slower until reaching equilibrium after 30 min and 3 h, respectively.

Adsorption steps. Detailed analysis of the observed dissipation changes per frequency unit shown in Fig. 2c, f make it possible to extract more information about the individual steps of the protein adsorption and different viscoelastic properties of the adsorbed protein layers. The adsorption of BSA on NDs is a two-step process. In Fig. 2c, the steeper slope in the first step compared to the second step indicates that the proteins most probably undergo small orientational changes after the attachment to the ND surfaces.[18, 33] The proteins orient differently because they have different elemental and charge distribution across their surfaces.

The adsorption process for LYS is more complicated on both types of NDs than for BSA. This can be clearly seen from the adsorption profiles in Fig. 2d-f. In the case of LYS on O-ND, the first derivative of the frequency with time reveals that LYS adsorption on O-ND is a three-step process (Fig. 2e): first layer formation (dip), second layer formation (dip) and dehydration (peak). The adsorption speed of the second LYS

layer is slightly slower than of the first layer. Interestingly, the mass of the second adsorbed LYS layer is nearly 2 times higher compared to the first layer. The dehydration process of LYS is also obvious from the sharp change in the Fig. 2e, where the dissipation decreases due to the removal of water from the adsorbed protein layers. The magnitude of dissipation changes is relatively small at all steps, suggesting that the adsorbed LYS layers are relatively rigid.

The adsorption process of LYS on H-ND is even more complicated than on O-ND. Even though, both LYS and H-ND are positively charged at the studied pH level, the adsorption still takes place. The Δf profile shows that the adsorption is a multi-step process, and it takes relatively long time to reach equilibrium (> 3 h). QCM spectra show signatures of a fast first layer formation, followed by slow multilayer adsorption and dehydration stages. The first monolayer formation is very similar to the fast adsorption of LYS on O-ND. The second layer (multilayers), however, forms after approximately 30 min and the mass is 3 times larger compared to the first monolayer. The magnitude of the observed dissipation changes is much larger than those measured on O-ND (Fig. 2f). This observation may be due to the multilayer formation or conformational changes of LYS on H-ND.

ATR-FTIR. Attenuated total reflection Fourier transform infrared spectroscopy (ATR-FTIR) is used to study the conformational changes in the protein structures before and after adsorption on H-ND and O-ND. The results of these measurements are shown in Fig. 3. The full FTIR spectrums can be found in Supplementary Information (Fig. S4†).

According to previous FTIR studies, the protein structure is derived from the shape and position of peaks of different amide bonds (amide I, II and III).[31, 34-36] Table 4 shows the results of the curve fitting analysis using amide I and II peaks in the FTIR spectra. The amide I region (1600-1700 cm^{-1}) has been widely used for studying conformational changes of different proteins.[34-36] The amide II region (1500-1600 cm^{-1}) is less sensitive compared to amide I, and it originates mainly from N-H in-plane bending and C-N stretching vibrations.[34] However, the amide I/II ratio has been identified as a good indicator of orientation changes of the relevant bonds and conformational changes in proteins.[31, 36]

Curve fitting analysis in Table 4 and Fig. 3 shows that both proteins undergo some structural changes in the backbone structure (α-helix, β-sheet/turn and random coils) after adsorption on different NDs. The observed conformational changes of BSA, however, are much smaller than of LYS.

BSA-ND complex: There is no apparent change observed in amide I position after adsorption of BSA on NDs, while amide II shifts by around 17±4 cm^{-1}. The change in amide I/II ratios are negligible for both H-ND and O-ND. α-helical structure is reduced by ~7-13%, and there is a slight increase in β-sheets/turns or random coils upon the adsorption. Therefore, the protein structure of BSA is only slightly modified by the interaction with both types of NDs. These minor conformational changes might also be due to the elongation of the protein near the ND surface (as discussed later).

LYS-ND complex: The amide I position is not changed significantly in LYS-ND complexes compared to pure LYS. However, the position of amide II shows a relatively large shift after the adsorption on NDs (up to 30±4 cm^{-1} for LYS and H-ND). The ratio of amide I/II intensity of LYS is much larger on NDs, indicating a significant reduction of amide II bonds. This means that LYS loses its predominant amide II structure upon the adsorption. The percentage of α-helices, β-sheets/turns or random coils derived from amide I peak suggests that the dominance of the α-helical structure is slightly reduced. FTIR spectra show that LYS undergoes some conformational changes on both H-ND and O-ND.

Discussion

Charge effects. Interaction forces between nanoparticles and proteins include van der Waals forces, hydrogen bonding, hydrophobic and electrostatic forces. From the thermodynamics point of view, the main binding forces can be derived using the full energy thermodynamic analysis of the reaction between proteins and the ND surfaces.[37, 38] The interactions between proteins and NDs are described by the change of the Gibbs free energy (ΔG) of the system, $\Delta G = \Delta H - T\Delta S$, where T is temperature and ΔS and ΔH are entropy and enthalpy changes, respectively.

At a constant temperature, the interaction between proteins and NDs leads to the penetration and disturbance of the hydration layers around the proteins (without conformational changes) and nanoparticles, which leads to an increase in the disorder of the solvent and an increase of the entropy of the system, i.e. $\Delta S > 0$.[37] When $\Delta S > 0$ and $\Delta H < 0$, the electrostatic forces are the major driving forces in the system because the other interactions have lower energies.[37, 38]

The negative changes in the enthalpy of the system ($\Delta H < 0$) in the adsorption of proteins (bone morphogenetic protein-2 (BMP-2)) on nanocrystalline diamond films have been recently determined by Kloss *et al.* using a combination of *ab initio* force-field-calculations and single molecule force spectroscopy measurements.[38] Theoretical calculations predicted that the contribution of electrostatic forces comprise around 75-80% of the total interaction of the proteins with oxygen (OH groups) and hydrogen-terminated nanocrystalline diamond films.[38] Based on this analysis and other reports,[21, 39-41] one can concluded that the electrostatic forces can reasonably be expected to dominate in protein interaction with NDs. Our results also suggest that electrostatic force play an important role in the adsorption process.

Although electrostatic forces are expected to play a key role in the adsorption process with NDs, a simple electrostatic attraction/repulsion model does not explain the observed interactions between the proteins and the charged ND particles (Fig. 2a-f). For example, the amount of negatively charged BSA at pH 7.0 adsorb to negatively charged O-ND is the same compared to positively charged H-ND, without demonstrating any significant conformational changes. Moreover, the adsorption rates of BSA on O-ND has been much faster than on H-ND (Fig. 2a,b).

For this reason, more nuanced electrostatic model of protein adsorption on NDs is presented below that takes into account not only electrostatic forces, but also water hydration layer interactions. This model predicts significant pH change near the charged ND surfaces. This change can qualitatively explain most of the observed adsorption behaviour of BSA and LYS on O-ND and H-ND.

A charged surface or particle in contact with a dielectric (water or any electrolyte) induces an electric field within the electrolyte.[42, 43] This causes counter-ions in the buffer solution to electrostatically attract to the charged surface, which leads to the formation of a screening layer (e.g. by Cl^- or Na^+ ions). The

distribution of the ion concentrations (c_i) at any distance from the charged surface is given by:[42]

$$c_i(x) = c_i^b \exp\left(-\frac{e\varphi(x)}{k_B T}\right), \quad (2)$$

where e is the electron charge, c_i^b is the ion concentration in the bulk solution, k_B is the Boltzmann constant, T is the temperature and $\varphi(x)$ is the potential energy at distant x from the surface. Due to the higher concentration of the counter-ions near the surface, pH near the surface (pH_s) differs from the pH of the solution bulk (pH_b). By taking the negative base 10 logarithm on both sides of Equation 2, one obtains:[42]

$$pH_s = pH_b + 0.434\frac{e\varphi_s}{k_B T}, \quad (3)$$

which is the relation between surface pH (pH_s) and the surface potential (ϕ_s). The potential at any distance from a charged surface can be estimated by using Gouy–Chapman theory (an electrical double layer theory).[44] According to this theory the density of the surface charge can be expressed as a function of the potential of the surface as:[44]

$$\sigma_s = -\sqrt{8RT\varepsilon_r\varepsilon_0 c_E}\sinh\left(\frac{e\varphi_s}{2k_B T}\right), \quad (4)$$

where R is the gas constant, c_E is the concentration of the electrolyte, ε_r and ε_0 are relative permittivity of the solution and permittivity of the vacuum, respectively.

To calculate the charge density, first the charge of the ND surfaces should be determined. This can be done experimentally by measuring zeta-potential (ζ) of the nanoparticles, which is related to the surface charge (z) at very low ionic concentrations (e.g. deionized water) as:[45]

$$z = \frac{e\zeta}{k_B T}\frac{d\times(1+\kappa\times d)}{\lambda_B}, \quad (5)$$

where d is the diameter of the particle, $\kappa = \sqrt{8\pi\lambda_B \times I_s \times N_A}$ is the inverse of Debye length and $\lambda_B = e^2/4\pi\varepsilon_r\varepsilon_0 k_B T$ is Bjerrum length (I_s is the ionic strength of the solution and N_A is the Avogadro's constant).[45]

The surface charge and density can be calculated using Equation 5. This allows us to determine the surface potential from Equation 4, and finally calculate the surface pH_s as a function of ζ using Equation 3.

Fig. 4 shows the relation of pH_s to zeta-potential of nanoparticles at low, medium and high ionic strengths (mol.Lit^{-1}). The graph reveals major changes of the surface pH_s near charged surfaces even at very low concentration of ions, such as exist in our experiments.

By using experimentally determined ζ values of NDs, one can see that the pH value near the surface of O-ND with ζ of -50 mV is very low (1-3), while it is very high (11-12) for H-ND with ζ of +49 mV. Since the pH_s near the surface of a charged particle is different from the pH of the bulk solution, this will significantly modify the interaction between the proteins and NDs.

Previous studies of proteins at different pH have reported that pH of the environment has a significant role on the protein structure, shape and charge.[25] It is thus reasonable to assume that the structure and charge of the proteins have been adopted according to the corresponding surface pH_s near the diamond nanoparticles.

The total charge of a protein is usually expressed with respect to its isoelectric point (*IEP*), i.e. pH at which the total charge of the protein is neutral. Previous studies have shown that *IEP* of BSA is around pH 5.5, meaning surface gets negatively charged at pH > IEP and positively charged at pH < *IEP*.[46] Similarly, the net charge of LYS has been found pH-dependent. At pH values below the *IEP* of 11, the positive charge of LYS dominates, while at higher pH LYS becomes slightly negatively charged.[17]

Since proteins contain different chemical functional groups due to the presence various primarily amino acids on the surface, it is very important to analyse how the charge of these individual groups is affected by the modified pH_s. This will allow more precise determination of the protein behaviour at the corresponding pH_s conditions. There have been identified 6 types of amino acids in BSA and LYS which are able to carry charges: Arginine, Histidine and Lysine carry positive charge, while Aspartate, Glutamate and Tyrosine are charged negatively.[17]

At pH of 1-3 (O-ND region), both BSA and LYS are positively charged due to protonation of amine groups (-NH_3^+).[17] In this pH region, Arginine, Histidine and Lysine carry positive charges, while the other amino acids remain almost neutral. At pH of 11-12 (H-ND region) BSA is negatively charged and LYS is almost neutral. Aspartate, Tyrosine and Glutamate carry negative charges, while Arginine, Histidine and Lysine are almost neutral in this pH region.

Based on the above analysis the unexpected adsorption of BSA and LYS on O-ND and H-ND can be qualitatively explained (Fig. 5). Due to the presence of strongly charged ND surfaces, the surface pH_s near NDs is different compared to pH of the bulk solution. This results in very high (11-12) and low (1-3) values of pH_s in the vicinity of the H-ND and O-ND surfaces, respectively, leading to a dramatic change of the total charge of the proteins.

Consequently, the originally assumed slightly negatively charged BSA at pH 7.0 becomes positively charged in O-ND solutions and negatively charged in H-ND solutions. Similarly, the originally assumed positively charged LYS at pH 7.0 becomes almost neutral in H-ND solutions and more positively charged in O-ND solutions. This pH_s-induced modification of protein charge explains the protein-nanodiamond interactions. The only exception to the simple electrostatic attraction model is the adsorption of LYS on H-ND, where LYS is close to the IEP, and therefore, it is expected to become deficient in charge.

For this reason, electrostatic force may not be the only dominant force involved in the adsorption process and other forces such as van der Waals attractions, hydrogen bonding and hydrophobic forces may also play a role. Since the attractive van der Waals forces are usually short-ranged within 2.5 nm distance (comparable to LYS dimensions), their energy is anticipated to be less than k_BT (comparable to the energy of fluctuations at room temperature), and hence they can be ruled out as the main driving forces in this situation.

As LYS contains many hydrophobic residues on its surface (~ 83% of the surface),[47] and also because H-ND is slightly hydrophobic, then the hydrophobic forces might play the key role in the adsorption process of LYS on H-ND. This is also in line with previous studies, suggesting that LYS interacts with hydrophobic surfaces via hydrophobic forces.[48, 49] However, electrostatic interactions cannot be completely ignored in the LYS and H-ND reaction. Electric forces can induce further structural transformation of the protein structure after LYS adsorbs on the hydrophobic surface. Conformational change of

LYS in H-ND solutions may indicate possibility of such combined hydrophobic and electrostatic interactions.

Within the both mentioned pH regions, BSA carries much more charge compared to LYS. For example, at pH 1-3, BSA possesses around 100 [e^+] charges, while LYS has only 20 [e^+] charges.[17] Therefore, near-surface electrostatic forces between BSA and ND are expected to be stronger at low and high pH compared to LYS and ND. This is consistent with the observation of the higher adsorption rates of BSA than LYS on O-ND (~5 times faster) and H-ND.

The main reason for the slower adsorption of BSA on H-ND surface compared to O-ND can possibly be stronger repulsion between BSA molecules at pH 11-12 than at pH 1-3, [17, 46, 50] which can lead to longer times for finding the lowest adsorption configuration on the surface with already pre-adsorbed proteins.

Protein configuration. Using the results of FTIR, QCM-D and the charge analysis a model is developed to show the protein structure and configuration on O-ND and H-ND surfaces (Fig. 6).

In the case of the adsorption of BSA on NDs, there are very similar amounts of adsorbed BSA on both O-ND and H-ND, around 1.5-1.8 of BSA per nanodiamond particle (corrected for the wet mass contribution).[18] Therefore, BSA forms monolayers on both O-ND and H-ND. Despite the similarities in the adsorbed amount of the proteins, there are some differences between the adsorbed structure and adsorption dynamics of BSA on O-ND and H-ND. Assuming that the adsorbed proteins on NDs adjust their structure according to the surface pH_s, structure of adsorbed BSA on H-ND and O-ND has been modified from its basic heart-shaped structure (with ~8×3×3 nm in size) at pH 7.0 (Fig. 5).[51] At pH < 3.5, such as near O-ND, BSA features an expanded structure (Fig. 5), while the structure of BSA on H-ND is expected to be similar to that observed at pH > 8.0.[51]

The exact structure of BSA at high pH has not been determined yet, but from our experiments we can anticipate that the BSA structure on H-ND gets slightly more elongated than the basic heart-shaped structure, but less than the expanded structure on O-ND. This is consistent with the results of FTIR experiments that showed BSA to partially lose some of its α-helical structure upon the adsorption (~ 7-13%) on both NDs.

Based on the rinsing experiment (from QCM – Fig. S3†) and the observation of lower dissipation changes for BSA on H-ND than on O-ND, it is concluded that the binding of BSA on H-ND is more rigid (higher shear modulus). The faster adsorption rate of BSA on O-ND than H-ND suggests that BSA charging is more effective at low pH rather than at higher pH values. The two-stage dissipation changes-per-frequency (Fig. 2c) shows a higher slope in the second stage, which might indicate that BSA molecules undergo small orientational changes to find their minimal energy configuration. This interpretation is consistent with another adsorption study of BSA on positively charged surfaces, which reported an increase in the ratio of $COO^-/NH2^+$ (charged groups in amino acids) as a consequence of BSA reorientation.[52]

The mechanism of adsorption of LYS on O-ND and H-ND is very different and more complex than of BSA. The adsorption of LYS on O-ND leads to a formation of a protein bilayer. The first monolayer has a lower mass (half) compared to the second layer (Fig. 6). The second layer forms much slower compared to the first layer, and its completion is accompanied by dehydration (mass loss). Since the electrostatic screening of the first formed LYS layer is not sufficient to completely neutralize the electric field from NDs, the second layer is formed (with a slower adsorption rate compared to the first layer). Even though the orientation angle cannot be predicted by our experiments, it is assumed that the first monolayer adsorbs with its "side-on" position and the second monolayer with higher mass adsorbs in an "end-on" configuration.[19] In this configuration the expected mass of the second layer would be twice the mass of the first dehydrated layer.

The binding process of LYS to H-ND is complex due to formation of protein multilayers, dehydration and conformational changes of the protein structure. Based on the adsorbed mass determined from QCM experiments (calculating the surface area of each step in the $\partial(\Delta f)/\partial t$ graph) LYS forms a trilayer on H-ND. The amount of LYS in the first monolayer is around 1/3 (0.6 ng mm^{-2}) of the protein mass in the subsequent layers (1 and 0.8 ng mm^{-2}). The trilayer formation is also supported by a very low stability of the final (third) LYS layer in the rinsing experiment (Fig. S3†). Even though, LYS has been considered as a structurally stable or "hard" protein,[53] some changes in the secondary structure of LYS are observed when adsorbed on H-ND.

The binding between the H-ND surface and the first LYS layer is determined by hydrophobic and electrostatic binding. Peptide chains attach to the hydrophobic H-ND surface with their hydrophobic sides, while hydrophilic chains face into the bulk solution.[46] Similar to the adsorption of LYS on O-ND, LYS adsorbs in the "end-on" form in the second and third layers on H-ND. The binding of LYS molecules in the second and third layers is very weak, which might suggest protein binding via amine interactions.[47]

Conclusions

In summary, the nanodiamond-protein interactions are investigated using QCM-D and FTIR. By using strongly positively (hydrogen-terminated) and negatively (oxygen-terminated) charged nanodiamond particles, we have carried a systematic study of the role of electrostatic interactions on the protein binding, adsorption kinetics and structure of BSA and LYS on nanodiamonds. This study demonstrates that the electrostatic forces dominate the adsorption dynamics, attachment and conformation of the proteins on charged NDs.

A simple electrostatic model is developed that can qualitatively describe the observed adsorption behaviour of BSA and LYS on charged ND surfaces in water. According to this model, the electric fields surrounding the charged nanoparticles cause a strong modification of pH near the ND surfaces, giving rise to very low (1-3) and high (11-12) local pH at O-ND and H-ND surfaces. This charge-induced change of the surface pH near the nanoparticles significantly affects the net protein charge, hydration layer and affinity to the nanodiamond surfaces. As a result, BSA becomes positively and negatively charged near the O-ND and H-ND, respectively, and LYS becomes positively charged near the O-ND surface and almost neutral near the H-ND surface. The presented electrostatic model qualitatively explains the attraction between the proteins and charged NDs, as well as the observed high adsorption rates and the resulting structures of BSA and LYS on H-ND and O-ND.

BSA adsorbs in a monolayer form on both ND types, but with a higher speed on O-ND and slower on H-ND due to the observed reorientation of the adsorbed BSA. The adsorption of LYS on NDs is slower and more complex compared to BSA, exhibiting intricate multistage adsorption profiles. Specifically, LYS forms a double layer on O-ND surfaces and trilayers on H-ND accompanied by conformational changes and dehydration of the proteins. The dehydration and conformational changes are due to the strong electrostatic interactions and hydrophobic effects.

The difference between the formation of multilayers of LYS (small rigid protein) with significant conformational changes and monolayers of albumin (large soft protein) with minor conformational changes on the charged nanoparticles is attributed to the size, rigidity and screening effects of the proteins. This study represents an important insight into the role of electrostatic interactions in the complex protein-nanoparticle system, providing a guide for further understanding of interactions of nanoparticles with biological matter. This may lead to various biomedical applications, such as drug delivery, sensing of cellular biomarkers, tissue engineering, and self-assembly of proteins into functional complexes.

Acknowledgements

We acknowledge financial support from the University of Melbourne research and CSIRO top-up scholarships. The authors wish to acknowledge research facility and technical assistance from the Nanostructured Interfaces and Materials Science Group (NIMS) led by Prof. Frank Caruso at the department of Chemical and Biomolecular Engineering, The University of Melbourne. This research was supported under Australian Research Council's Discovery Projects funding scheme (project number DE120101100). K.O acknowledges support from the ARC Future Fellowship and CSIRO OCE Science Leadership Scheme.

Notes and references

[a] School of Physics, The University of Melbourne, Melbourne, Victoria 3010, Australia.
[b] School of Physics and Advanced Materials, University of Technology, Sydney, New South Wales 2007, Australia.
[c] Plasma Nanoscience Laboratories, Commonwealth Scientific and Industrial Research Organisation (CSIRO), PO Box 218, Lindfield, NSW 2070, Australia.
[d] School of Chemistry, Physics, and Mechanical Engineering, Queensland University of Technology, Brisbane QLD 4000, Australia.

* Corresponding authors:
mrtz.aramesh@gmail.com

† Electronic Supplementary Information (ESI) available: FTIR spectrum of nanodiamonds, QCM-D profiles of 50 nm nanodiamond adsorption on silica surfaces, QCM-D profiles of protein desorption after rinsing with water (rinsing experiment) and full FTIR spectrum of proteins before and after adsorption on ND particles. See DOI: 10.1039/b000000x/

References

1 L. P. McGuinness, Y. Yan, A. Stacey, D. A. Simpson, L. T. Hall, D. Maclaurin, S. Prawer, P. Mulvaney, J. Wrachtrup, F. Caruso, R. E. Scholten and L. C. Hollenberg, *Nat Nanotechnol*, 2011, **6**, 358.
2 T. J. Wu, Y. K. Tzeng, W. W. Chang, C. A. Cheng, Y. Kuo, C. H. Chien, H. C. Chang and J. Yu, *Nat Nanotechnol*, 2013, **8**, 682.
3 M. A. Zurbuchen, M. P. Lake, S. A. Kohan, B. Leung and L. S. Bouchard, *Sci Rep*, 2013, **3**, 2668.
4 V. N. Mochalin, O. Shenderova, D. Ho and Y. Gogotsi, *Nat Nanotechnol*, 2012, **7**, 11.
5 X. Q. Zhang, M. Chen, R. Lam, X. Y. Xu, E. Osawa and D. Ho, *ACS nano*, 2009, **3**, 2609.
6 M. Chen, E. D. Pierstorff, R. Lam, S. Y. Li, H. Huang, E. Osawa and D. Ho, *ACS nano*, 2009, **3**, 2016.
7 E. K. Chow, X. Q. Zhang, M. Chen, R. Lam, E. Robinson, H. Huang, D. Schaffer, E. Osawa, A. Goga and D. Ho, *Sci Transl Med*, 2011, **3**, 73ra21.
8 V. Vaijayanthimala, P. Y. Cheng, S. H. Yeh, K. K. Liu, C. H. Hsiao, J. I. Chao and H. C. Chang, *Biomaterials*, 2012, **33**, 7794.
9 K. K. Liu, C. C. Wang, C. L. Cheng and J. I. Chao, *Biomaterials*, 2009, **30**, 4249.
10 V. Petráková, A. Taylor, I. Kratochvílová, F. Fendrych, J. Vacík, J. Kučka, J. Štursa, P. Cígler, M. Ledvina, A. Fišerová, P. Kneppo and M. Nesládek, *Adv. Funct. Mater.*, 2012, **22**, 812.
11 A. Krueger and D. Lang, *Adv. Funct. Mater.*, 2012, **22**, 890.
12 M. Mahmoudi, I. Lynch, M. R. Ejtehadi, M. P. Monopoli, F. B. Bombelli and S. Laurent, *Chem. Rev.*, 2011, **111**, 5610.
13 Q. Mu, G. Jiang, L. Chen, H. Zhou, D. Fourches, A. Tropsha and B. Yan, *Chem. Rev.*, 2014, **114**, 7740.
14 M. Mahmoudi and V. Serpooshan, *The Journal of Physical Chemistry C*, 2011, **115**, 18275.
15 F. Meder, S. Kaur, L. Treccani and K. Rezwan, *Langmuir*, 2013, **29**, 12502.
16 A. A. Vertegel, R. W. Siegel and J. S. Dordick, *Langmuir*, 2004, **20**, 6800.
17 K. Rezwan, L. P. Meier and L. J. Gauckler, *Biomaterials*, 2005, **26**, 4351.
18 M. M. Ouberai, K. Xu and M. E. Welland, *Biomaterials*, 2014, **35**, 6157.
19 K. Xu, M. M. Ouberai and M. E. Welland, *Biomaterials*, 2013, **34**, 1461.
20 W. Yang, O. Auciello, J. E. Butler, W. Cai, J. A. Carlisle, J. E. Gerbi, D. M. Gruen, T. Knickerbocker, T. L. Lasseter, J. N. Russell, Jr., L. M. Smith and R. J. Hamers, *Nat Mater*, 2002, **1**, 253.
21 R. Hoffmann, A. Kriele, H. Obloh, N. Tokuda, W. Smirnov, N. Yang and C. E. Nebel, *Biomaterials*, 2011, **32**, 7325.
22 H. J. Huang, E. Pierstorff, E. Osawa and D. Ho, *ACS nano*, 2008, **2**, 203.
23 W. S. Yeap, Y. Y. Tan and K. P. Loh, *Anal. Chem.*, 2008, **80**, 4659
24 E. Perevedentseva, P. J. Cai, Y. C. Chiu and C. L. Cheng, *Langmuir*, 2011, **27**, 1085.
25 T. Peters Jr, in *All About Albumin*, ed. T. Peters, Academic Press, San Diego1995, pp. 9.
26 W. Norde and C. E. Giacomelli, *J. Biotechnol.*, 2000, **79**, 259.
27 O. Shimoni, J. Cervenka, T. J. Karle, K. Fox, B. C. Gibson, S. Tomljenovic-Hanic, A. D. Greentree and S. Prawer, *ACS Appl Mater Interfaces*, 2014, **6**, 8894.

28 F. Höök, M. Rodahl, P. Brzezinski and B. Kasemo, *Langmuir*, 1998, **14**, 729.
29 Sabine Hauck, Stephan Drost, Elke Prohaska, Hans Wolf and S. Dübel, in *Protein–Protein Interactions: A Molecular Cloning Manual*, Cold Spring Harbor Laboratory Press2002, ch. 15, pp. 273.
30 M. Karlsson, *J. Biol. Chem.*, 2005, **280**, 25558.
31 P. Roach, D. Farrar and C. C. Perry, *J. Am. Chem. Soc.*, 2005, **127**, 8168.
32 H. D. Wang, C. H. Niu, Q. Yang and I. Badea, *Nanotechnology*, 2011, **22**, 145703.
33 Y. F. Yano, *J Phys Condens Matter*, 2012, **24**, 503101.
34 V. Militello, C. Casarino, A. Emanuele, A. Giostra, F. Pullara and M. Leone, *Biophys. Chem.*, 2004, **107**, 175.
35 A. Barth, *Biochim. Biophys. Acta*, 2007, **1767**, 1073.
36 P. Roach, D. Farrar and C. C. Perry, *J. Am. Chem. Soc.*, 2006, **128**, 3939.
37 P. D. Ross and S. Subramanian, *Biochemistry*, 1981, **20**, 3096.
38 F. R. Kloss, R. Gassner, J. Preiner, A. Ebner, K. Larsson, O. Hachl, T. Tuli, M. Rasse, D. Moser, K. Laimer, E. A. Nickel, G. Laschober, R. Brunauer, G. Klima, P. Hinterdorfer, D. Steinmuller-Nethl and G. Lepperdinger, *Biomaterials*, 2008, **29**, 2433.
39 E. Ōsawa, D. Ho, H. Huang, M. V. Korobov and N. N. Rozhkova, *Diamond Relat. Mater.*, 2009, **18**, 904.
40 A. Adnan, R. Lam, H. Chen, J. Lee, D. J. Schaffer, A. S. Barnard, G. C. Schatz, D. Ho and W. K. Liu, *Mol Pharm*, 2011, **8**, 368.
41 T. Lechleitner, F. Klauser, T. Seppi, J. Lechner, P. Jennings, P. Perco, B. Mayer, D. Steinmuller-Nethl, J. Preiner, P. Hinterdorfer, M. Hermann, E. Bertel, K. Pfaller and W. Pfaller, *Biomaterials*, 2008, **29**, 4275.
42 R. A. Hartvig, M. van de Weert, J. Ostergaard, L. Jorgensen and H. Jensen, *Langmuir*, 2011, **27**, 2634.
43 V. Chakrapani, J. C. Angus, A. B. Anderson, S. D. Wolter, B. R. Stoner and G. U. Sumanasekera, *Science*, 2007, **318**, 1424.
44 V. S. Bagotsky, *Fundamentals of Electrochemistry: Second Edition*2005.
45 S. K. Sainis, J. W. Merrill and E. R. Dufresne, *Langmuir*, 2008, **24**, 13334.
46 L. R. Barbosa, M. G. Ortore, F. Spinozzi, P. Mariani, S. Bernstorff and R. Itri, *Biophys. J.*, 2010, **98**, 147.
47 D. Nepal and K. E. Geckeler, *Small*, 2006, **2**, 406.
48 D. Nepal and K. E. Geckeler, *Small*, 2007, **3**, 1259.
49 G. Zuo, S. G. Kang, P. Xiu, Y. Zhao and R. Zhou, *Small*, 2013, **9**, 1546.
50 S. Staunton and H. Quiquampoix, *J. Colloid Interface Sci.*, 1994, **166**, 89.
51 E. Edri and O. Regev, *Anal. Chem.*, 2008, **80**, 4049.
52 X. N. Hu and B. C. Yang, *J Biomed Mater Res A*, 2014, **102**, 1053.
53 C. A. Haynes and W. Norde, J. Colloid Interface Sci., 1995, 169, 313.

Figures:

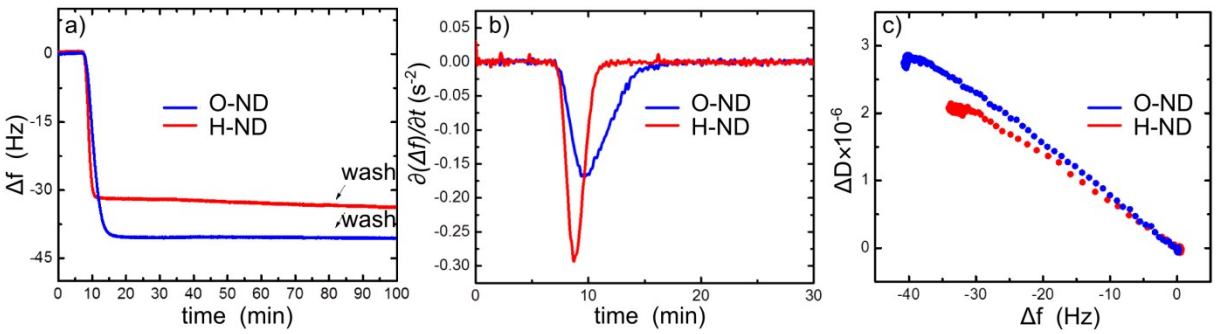

Fig. 1. QCM-D profiles of H-ND and O-ND adsorption on silica surfaces. a) the frequency shifts, b) the first derivative of the frequency shifts and c) the dissipation changes per frequency units.

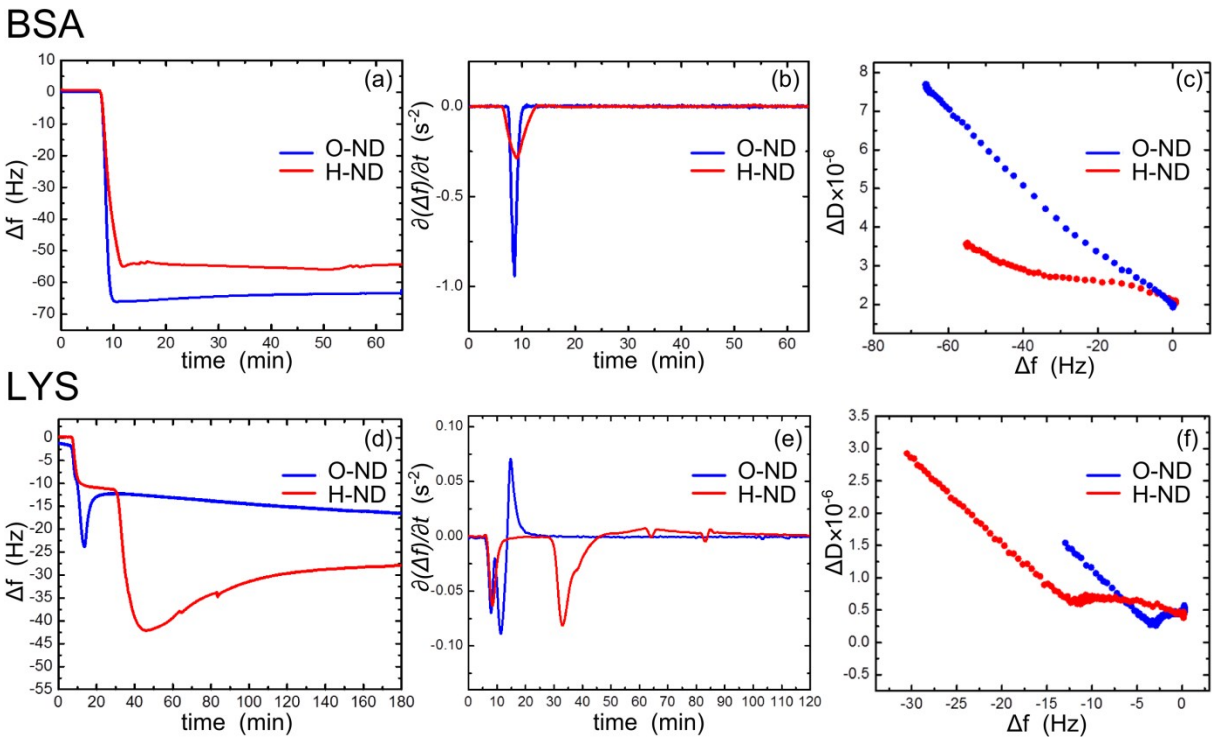

Fig. 2. QCM-D profiles of BSA (top) and LYS (bottom) protein adsorption on ND surface using frequency (Δf) and dissipation (ΔD) monitoring as a function of time. a,d) the frequency shifts, b,e) the first derivative of the frequency shifts and c,f) the dissipation changes per frequency units.

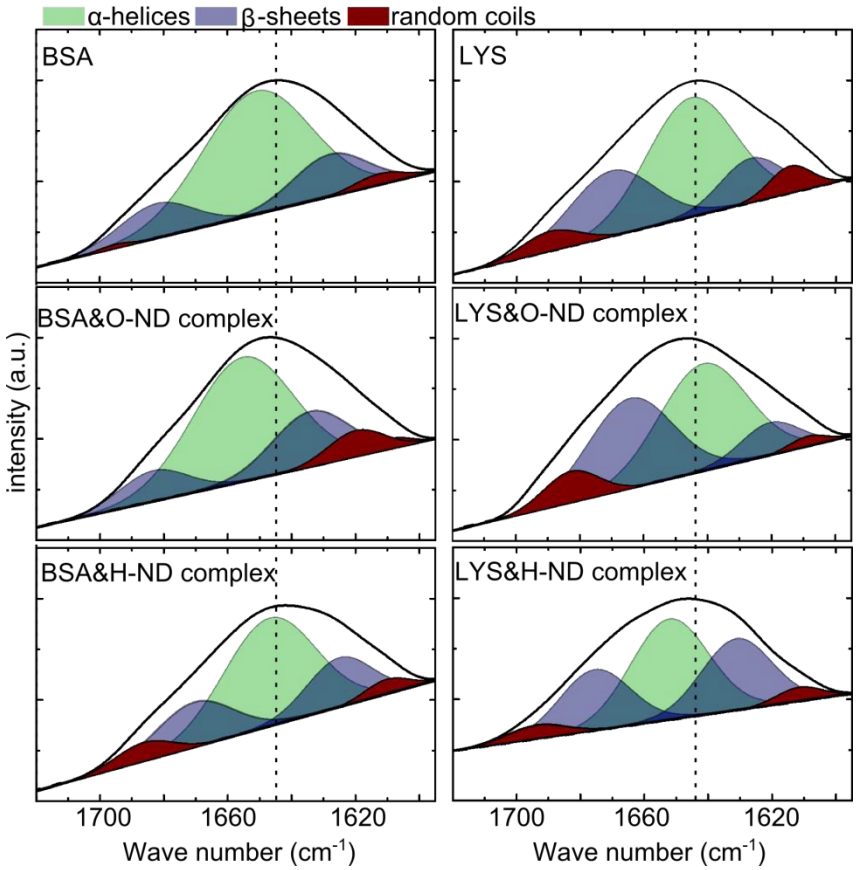

Fig. 3. FTIR spectra of amide I region of BSA (top) and LYS (bottom) proteins before and after adsorption on O-ND and H-ND particles.

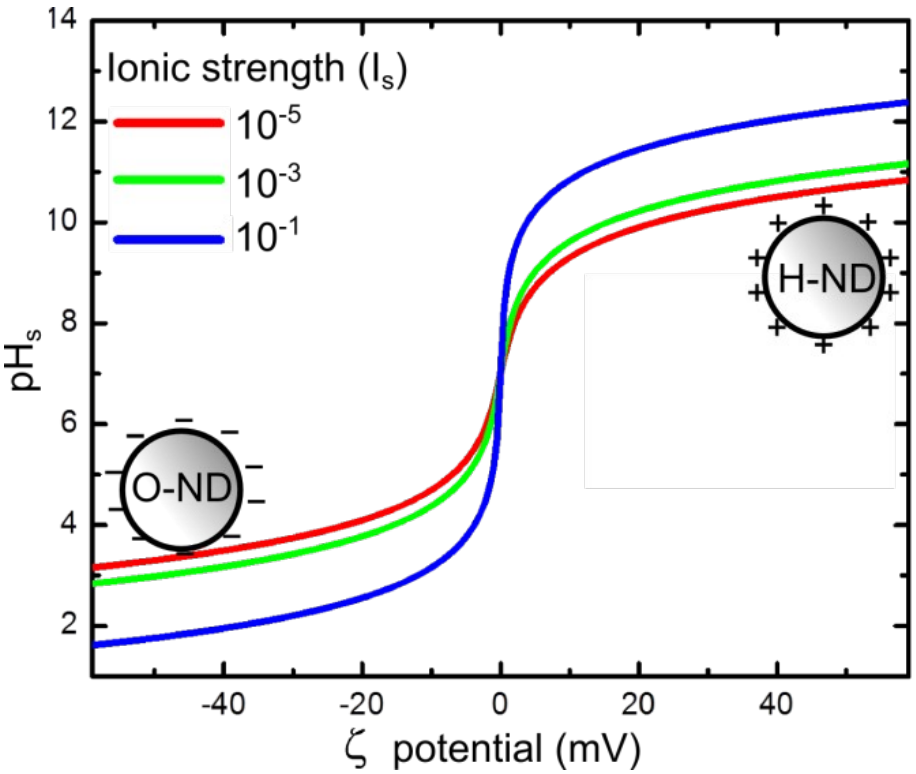

Fig. 4. Surface pH as a function of ζ for solutions with different ionic strength (mol.Lit^{-1}).

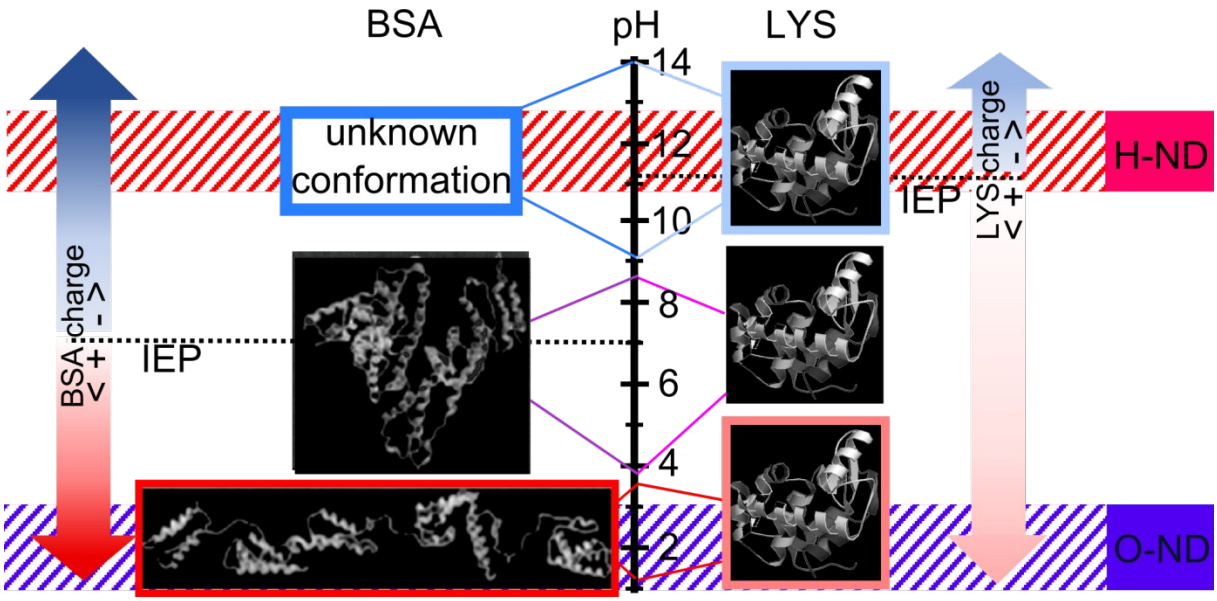

Fig. 5. Structure and charge of BSA (left) and LYS (right) under different pH conditions. [17, 25, 47]

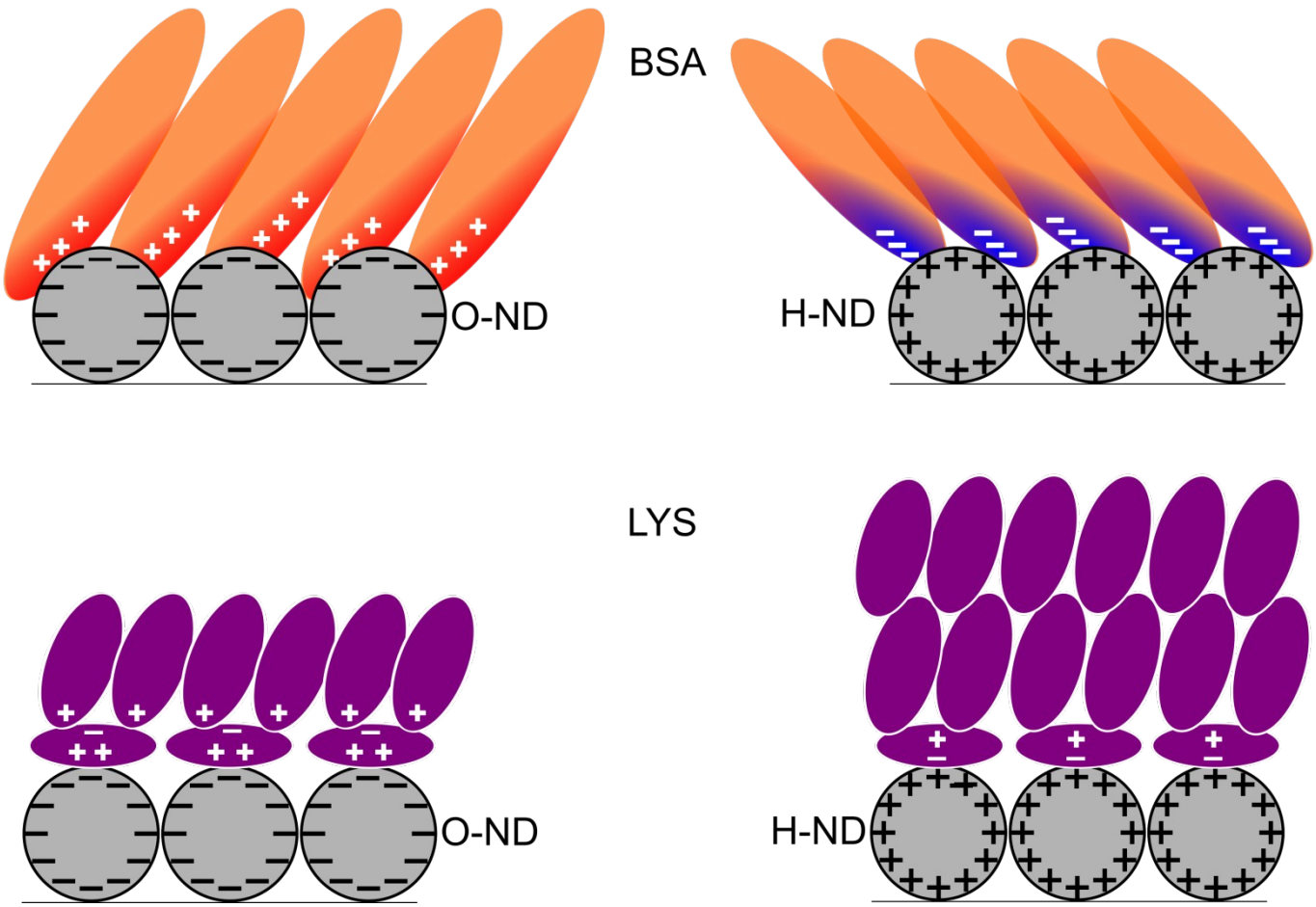

Fig. 6. Models of protein adsorption configurations of BSA (top) and LYS (bottom) on O-ND (left) and H-ND (left) surfaces. The size and ratio of the proteins and particles are in scale and as determined from the QCM data. (*n.b.* The first monolayers of LYS on H-ND and O-ND are shown thinner due to the significant protein dehydration)

Tables:

ND type	Size (nm)	ζ (mV)
As received	198±69	-32±5
O-terminated (O-ND)	5±1	-51±2
H-terminated (H-ND)	5±1	+49±2

Table 1. ND characteristics measured with dynamic light scattering (DLS) measurements.

ND type	Substrate	- Δf_{ads} (Hz)	ΔD_{ads}	$mass_{ads}$ (ng)	$Number_{ads}$	$-\Delta f_{des}$ (Hz)	ΔD_{des}	$mass_{des}$ (ng)
O-	SiO_2	41.0	2.80	242	$1.8\pm0.3 \times 10^{12}$	0	0.06	0
H-	SiO_2	34.4	2.04	203	$1.5\pm0.3 \times 10^{12}$	0	0.11	0

Table 2. ND deposition parameters on silica surface determined from QCM-D graphs.

Δf_{ads}: frequency shifts upon adsorption of NDs, ΔD_{ads}: energy dissipation changes upon adsorption of NDs, $mass_{ads}$: mass of the adsorbed ND layer, $Number_{ads}$: number of the adsorbed ND particles, Δf_{des}: frequency shifts upon rinsing with water, ΔD_{des}: energy dissipation changes upon rinsing with water, $mass_{des}$: mass of the desorbed NDs upon rinsing.

Protein	Substrate	$-\Delta f_{ads}$ (Hz)	ΔD_{ads}	$mass_{ads}$ (ng)	$Number_{ads}$	$-\Delta f_{des}$ (Hz)	ΔD_{des}	$mass_{des}$ (ng)	$Number_{des}$
BSA	SiO_2	28.1	1.76	165	1.5×10^{12}	-5.1	-1.36	-30	2.7×10^{11}
BSA	O-	63.4	5.73	374	3.4×10^{12}	-4.0	-2.62	-24	2.1×10^{11}
BSA	H-	53.3	3.39	314	2.9×10^{12}	-3.3	-1.66	-19	1.7×10^{11}
LYS	SiO_2	11.1	2.50	65	2.7×10^{12}	-16.3	-2.5	-96	4.0×10^{12}
LYS	O-	22.0	0.42	130	5.4×10^{12}	-6.7	-0.74	-40	1.7×10^{12}
LYS	H-	42.2	3.41	249	1.0×10^{13}	-26.2	-0.79	-155	6.5×10^{12}

Table 3. Protein adsorption parameters of BSA and LYS on different ND-coated substrates obtained from QCM-D.

Δf_{ads}: frequency shifts upon adsorption of proteins, ΔD_{ads}: energy dissipation changes upon adsorption of proteins, $mass_{ads}$: mass of the adsorbed protein layer, $Number_{ads}$: number of the adsorbed proteins, Δf_{des}: frequency shifts upon rinsing with water, ΔD_{des}: energy dissipation changes upon rinsing with water, $mass_{des}$: mass of the desorbed proteins upon rinsing.

Protein	ND type	Amide I position (cm^{-1})	Amide II position (cm^{-1})	Amide I/II intensity ratio	α-Helices (%)	β-sheets/ turns (%)	Random coil (%)
BSA	-	1644	1517	1.018	67.84	28.42	3.74
BSA	O-	1644	1535	1.039	60.41	30.11	9.48
BSA	H-	1644	1532	1.015	54.32	35.99	9.69
LYS	-	1643	1516	1.132	49.60	38.17	12.23
LYS	O-	1646	1532	1.260	44.09	44.19	11.72
LYS	H-	1646	1546	1.639	41.52	49.15	9.33

Table 4. FTIR analysis of proteins before and after adsorption on ND particles.

